# The Pulsed Coherent Doppler Lidar: Observations of Frontal Structure and the Planetary Boundary Layer

PAUL J. NEIMAN

*Cooperative Institute for Research in Environmental Sciences, University of Colorado/NOAA, Boulder, Colorado*

M. A. SHAPIRO, R. MICHAEL HARDESTY, B. BOBA STANKOV, RHIDIAN T. LAWRENCE, ROBERT J. ZAMORA, AND TAMARA HAMPEL

*NOAA/ERL/Wave Propagation Laboratory, Boulder, Colorado*

(Manuscript received 28 August 1987, in final form 22 February 1988)

ABSTRACT

The NOAA/WPL pulsed coherent Doppler lidar was used during the Texas Frontal Experiment in 1985 to study mesoscale preconvective atmospheric conditions. On 22 April 1985, the Doppler lidar, in conjunction with serial rawinsonde ascents and National Weather Service rawinsonde ascents, observed atmospheric features such as middle-tropospheric frontal and vertical wind shear layers and the planetary boundary layer. The lidar showed unique evidence of the downward transport of strong winds from an elevated vertical speed shear (frontal) layer into the planetary boundary layer. The lidar provided further evidence of atmospheric processes such as clear-air turbulence within frontal layers, and dry convection turbulence within the superadiabatic planetary boundary layer. As a result, high-technology remote sensing instruments such as the Doppler lidar show considerable promise for future studies of small-scale weather systems in a nonprecipitating atmosphere.

## 1. Introduction

Since the early 1980s the National Oceanic and Atmospheric Administration/Wave Propagation Laboratory (NOAA/WPL) has operated a pulsed Doppler lidar in remote sensing field exercises to obtain a better understanding of selected mesoscale and turbulent-scale meteorological phenomena such as microbursts (Rothermel et al. 1985), dryline circulations (Parsons et al. 1986), and canyon winds (Post and Neff 1986). The current study presents an analysis of lidar data and conventional rawinsonde data taken during the NOAA/WPL Texas Frontal Experiment (TEXEX). TEXEX took place at the National Weather Service (NWS) Office at Midland, Texas, from 15 April to 31 May 1985. The primary objective of the field experiment was to examine the short-term (<6 h) evolution of mesoscale pre-convective conditions over west Texas.

The current study describes the pertinent weather features affecting Texas on 22 April 1985 in synoptic-scale and lidar analyses. On this day, Midland was under the influence of post-cold-frontal conditions. Observations were made of midtropospheric frontal features and the downward transport of momentum in the planetary boundary layer (PBL). High-frequency monitoring of temperature through these frontal features was realized from serial rawinsonde ascents. The unique capabilities of the Doppler lidar provided detailed observations of the high-frequency ($\geq$1 s) evolution and turbulent-scale structure of winds in the midtropospheric frontal features and the PBL. The lidar measured vertical wind shear within the frontal layers and the high-frequency motions arising from clear air turbulence (CAT) in the vicinity of these fronts. The lidar also measured horizontal and vertical winds and the downward transport of momentum within the PBL.

## 2. The Doppler lidar

The WPL pulsed coherent Doppler lidar emits electromagnetic energy at an infrared wavelength of 10.6 $\mu$m. This energy is scattered from aerosols with a characteristic diameter of $\sim$1–3 $\mu$m (Post et al. 1978). The greater the density of aerosols in an atmospheric layer, the stronger the return signal. Since the lidar beam is severely attenuated by water droplets found in clouds, the device is employed primarily for studies of clear-air phenomena. Post et al. (1981) and Hardesty et al. (1983) offer a more complete description of performance characteristics on the Doppler lidar.

The lidar collected data utilizing a variety of scans. Vertical motions were measured by directing the lidar beam vertically, while cross sections of radial wind were obtained by range-height-indicator (RHI) scans. Sim-

*Corresponding author address:* Paul J. Neiman, CIRES, University of Colorado/NOAA, Boulder, CO 80309.

ilarly, plan-position-indicator (PPI) scans showed circum-azimuthal slices of radial velocity at a fixed elevation angle. Vertical profiles of horizontal winds were determined by applying the Velocity Azimuth Display (VAD) technique (Browning and Wexler 1968) to the PPI scan at fixed range gates. Lidar wind measurements using this technique have been shown to agree with tower wind measurements to within better than 1 m $s^{-1}$ (Hall et al. 1984) when the mean wind was uniform across the cone scanned by the lidar.

### 3. Data acquisition and processing

The lidar-derived time–height section ($t$, $z$) of horizontal winds was prepared by combining three different datasets. The first dataset consisted of 10 VAD wind profiles between 1442 and 2050 UTC, obtained at an elevation scan angle of 60 degrees (Fig. 1). The lowest range gate was 1290 m AGL; a 300 m range gate interval corresponded to a 258 m vertical resolution. The second dataset consisted of five VAD profiles between 1517 and 1826 UTC, obtained at an elevation scan angle of 10 degrees (Fig. 2). The lowest range gate was 259 m AGL with a vertical resolution of 51 m. The third dataset consisted of seven surface observations from Midland, Texas (Fig. 3). The combined dataset was subjected to two passes of a 4253EHT nonlinear median filter (described by Velleman and Hoaglin 1981), first with respect to time, then with respect to height. The filter was implemented to eliminate instrument-induced spurious data and remove very-small-scale natural atmospheric variability while retaining larger-scale structure. Finally, Lanczos' (1956) low-pass filter was applied to the horizontal wind time series, using a cutoff frequency of 30 minutes. The 1200 UTC Midland synoptic rawinsonde wind profile was added to the time–height section.

The lidar also measured vertical velocity ($W$) when the beam was placed in a vertical direction. The sampling rate for $W$ was 1 Hz for 1073 consecutive seconds starting at 1724 UTC and ending at 1742 UTC. The lidar measured vertical motions between 1.95 and 6.15 km AGL, inclusive, at intervals of 0.3 km. These data were edited and filtered like the VAD dataset. No Lanczos filter was applied. Spectral analysis was performed on each of the $W$ time series. Then, vertical profiles of vertical velocity variance were plotted for designated groups of frequencies.

A time–height section of virtual potential temperature ($\theta_v$) was created using five rawinsonde launches (1443 UTC, 1535 UTC, 1730 UTC, 1927 UTC and 2103 UTC) and the 1200 UTC Midland synoptic rawinsonde launch. The soundings within the $\theta_v$ time–height section were temporally adjusted to take into account the difference between initial launch time and the time of $\theta_v$ measurements aloft; an average rawin-

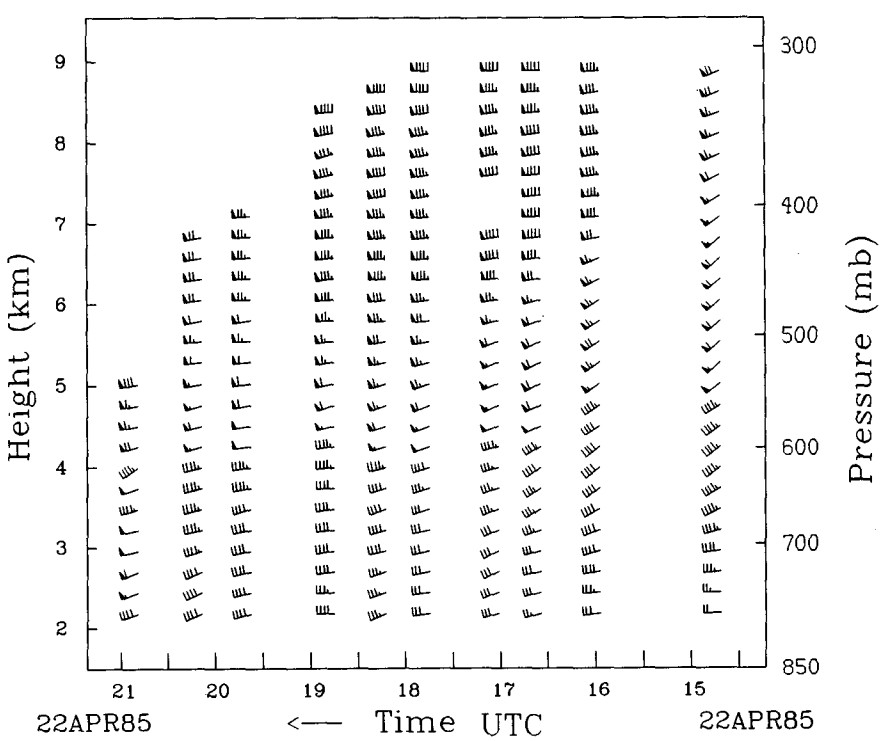


FIG. 1. Time–height section of horizontal winds at Midland, Texas measured by the NOAA/WPL Doppler lidar from 1442 to 2050 UTC 22 April 1985 using an elevation scan angle of 60 degrees (flag: 25 m $s^{-1}$, barb: 5 m $s^{-1}$, half barb: 2.5 m $s^{-1}$).

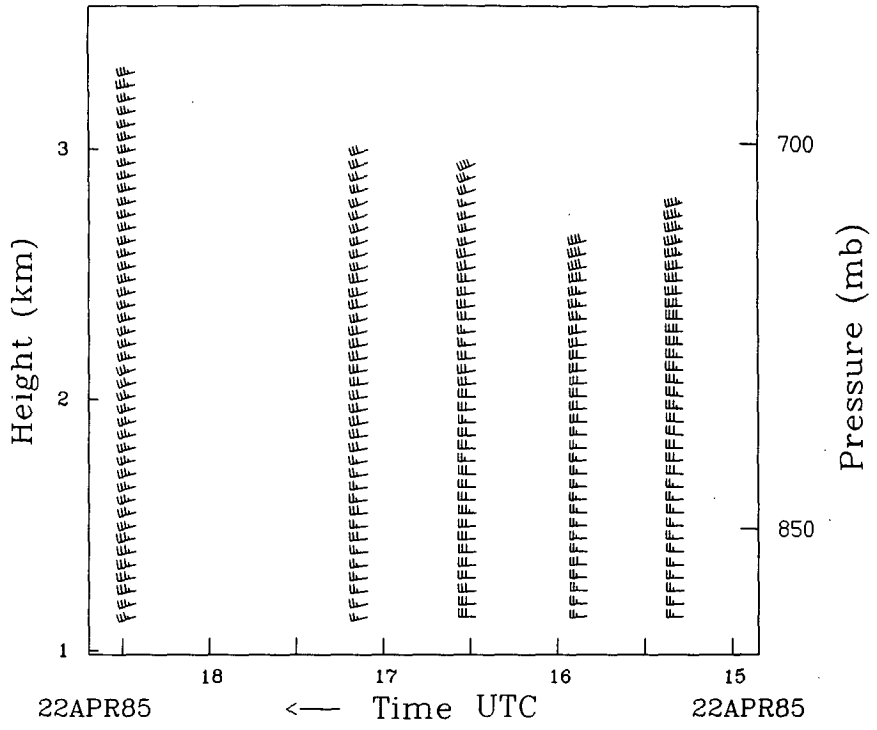


FIG. 2. Time–height section of horizontal winds measured by the Doppler lidar from 1517 to 1826 UTC 22 April 1985 using an elevation scan angle of 10 degrees. Wind vectors are as described in Fig. 1.

sonde ascent rate of 0.3048 km $min^{-1}$ was assumed. Two cross sections of $\theta_v$, winds, and mixing ratio, $r$, were constructed using the 1200 UTC 22 April NWS synoptic rawinsonde network.

## 4. Synoptic overview

On 21 April 1985, a synoptic-scale trough was located over the western half of the United States. During the period 0000–1200 UTC 22 April, a 300 mb jet stream maxima propagated east-southeastward into the base of the trough and conributed to the sharpening of the upper-level wavelength over Colorado by 0000 UTC 23 April (Fig. 4). The surface cyclone over Kansas deepened from 998 mb at 1200 UTC 22 April to 995 mb at 2100 UTC in response to the approaching upper-level short wave and its associated vorticity maximum.

At 1200 UTC 22, a short wave in the 500 mb temperature and wind fields was west of Midland; southwest winds were observed over Midland (Fig. 5). As the short wave translated eastward during the following 12 hours, the 500 mb wind over Midland veered to almost due west (Fig. 6). The 500 mb temperature at Midland increased 4°C between 1200 UTC 22 and 0000 UTC 23 as the thermal short-wave trough axis moved eastward into eastern Texas. The 700 mb temperature and wind fields behaved in a similar manner. At 1200 UTC 22, the 850 mb thermal field contained a significant temperature gradient [~2.5°C (100 km)$^{-1}$] between Midland and El Paso. By 0000 UTC 23 April, no significant west–east temperature gradient was observed across Texas from Longview to El Paso. Differential diabatic heating, $\partial(d\theta/dt)/\partial x$, described by Miller (1948) and Saucier (1955) played a significant role in the observed frontolysis. Strong solar insolation in the cloud-free region west of the cold front resulted in significant warming and dry convective overturning, whereas little diurnal temperature variation occurred under the cloud cover and in the ample moisture east of the front. The differential west–east heating diminished the low-level west–east frontal baroclinity by late

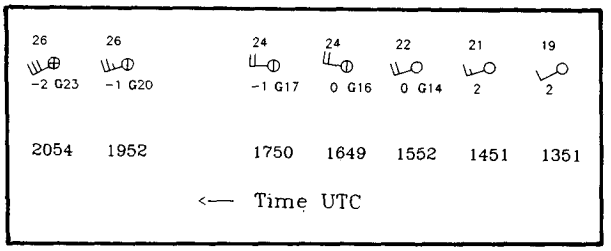


FIG. 3. Hourly surface observations at Midland, Texas from 1351 to 2054 UTC 22 April 1985. The temperature and dewpoint (°C) for each hour are found in the upper and lower left portions of the station plots, respectively. Wind gusts (m $s^{-1}$), if any, are noted in the lower right part of each station plot. Wind vectors are as described in Fig. 1.

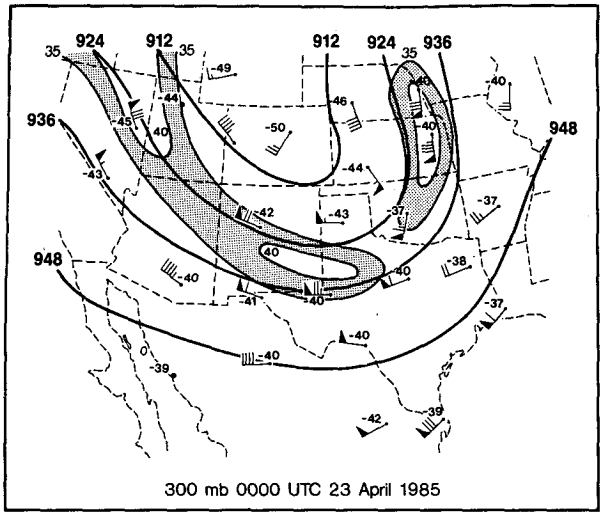


FIG. 4. The 300 mb height ($m \times 10$, heavy lines) and wind speed (m $s^{-1}$, thin lines) at 0000 UTC 23 April 1985. The area with 35 to 40 m $s^{-1}$ wind speed is stippled. The temperatures (°C) are plotted in the upper left portion of the station plots. Wind vectors are as described in Fig. 1.

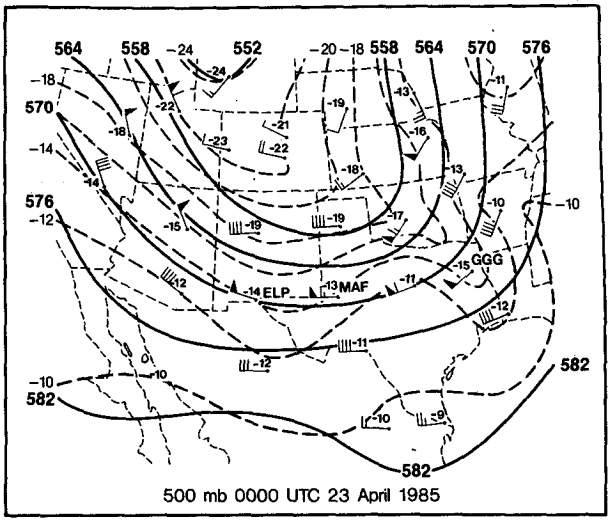


FIG. 6. The 500 mb height ($m \times 10$) and temperature (°C) at 0000 UTC 23 April 1985. Temperatures (°C) are plotted in the upper left portion of the station plots. Wind vectors are as described in Fig. 1. ELP: El Paso; MAF: Midland; and GGG: Longview, Texas.

afternoon (0000 UTC 23). The boundary was reduced to a moisture and wind shift discontinuity.

Despite the lack of a strong surface pressure gradient at 1800 UTC 22 April, there were sustained westerly winds of 10–25 m $s^{-1}$ from Amarillo to Midland to Guadalupe Pass, Texas (Fig. 7). Strong west winds were probably being transported down toward ground level by dry convection in the clear air behind the cold front in conjunction with a significant vertical speed shear layer capping the PBL (~15 m $s^{-1}$/km, shown in §5). The downward transport of strong westerly winds contributed to the development of deep moist convection by strengthening the boundary layer wind component normal to and behind the front or dryline, thus enhancing frontal or dryline convergence in the lower

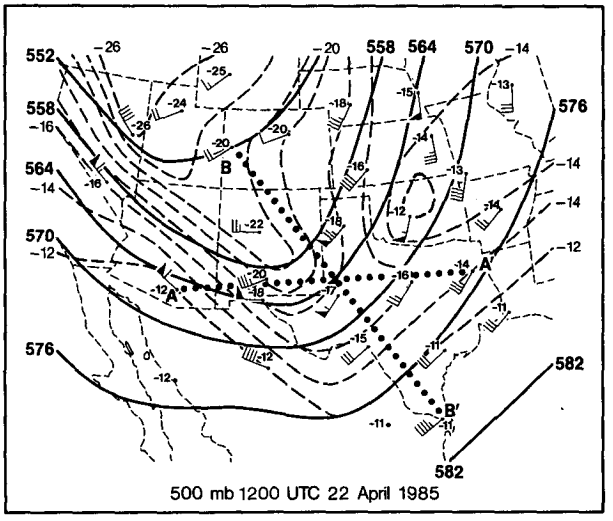


FIG. 5. The 500 mb height ($m \times 10$) and temperature (°C, dashed lines) at 1200 UTC 22 April 1985. The temperatures (°C) are plotted in the upper left portion of the station plots. Wind vectors are as described in Fig. 1. Lines AA′ and BB′ are projection lines for Figs. 9 and 10 cross sections, respectively.

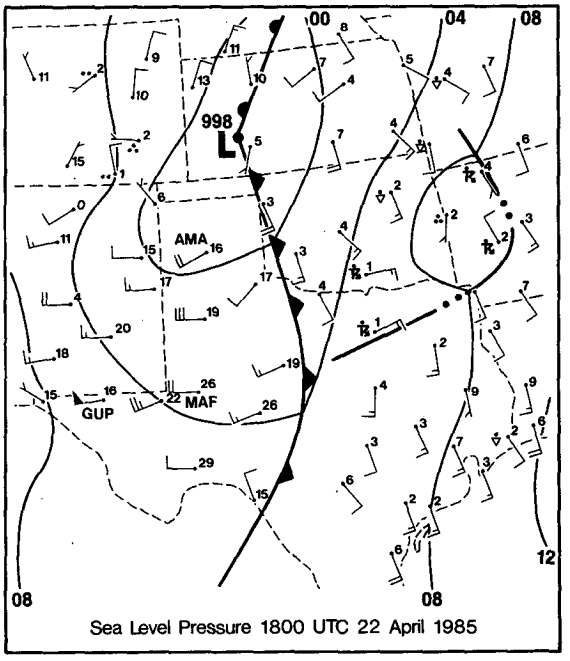


FIG. 7. Sea level pressure analysis (mb) with surface dewpoint temperature depression (°C) and wind vectors at 1800 UTC 22 April 1985. Dewpoint depressions (°C) are plotted in the upper right portion of the station plots. Wind vectors are as described in Fig. 1. GUP: Guadalupe Pass and AMA: Amarillo, Texas.

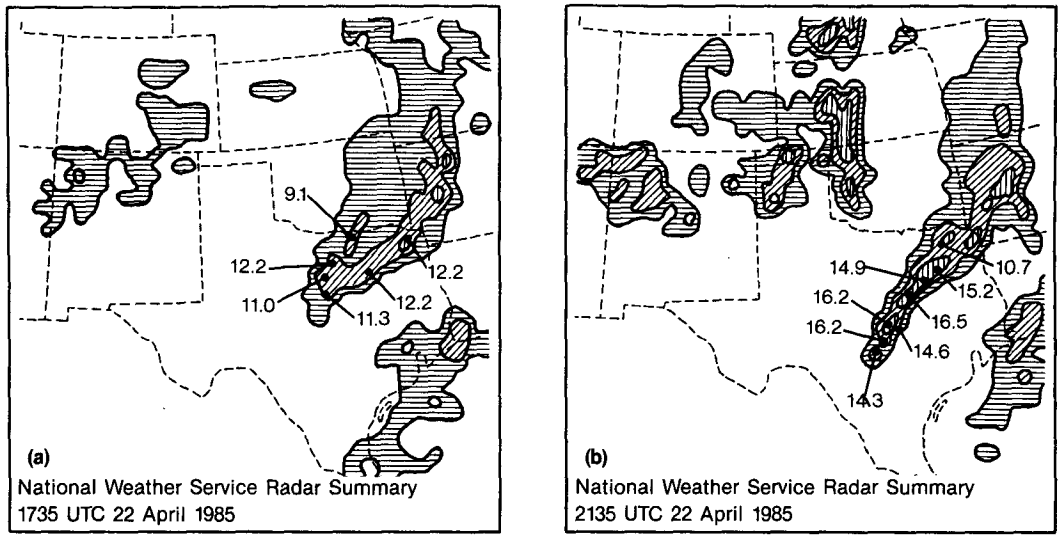


FIG. 8. National Weather Service (NWS) radar summary for (a) 1735 UTC 22 April 1985, and (b) 2135 UTC 22 April 1985. Heights of precipitation cells are in kilometers.

troposphere. Other factors may also have contributed to the deep convection. Diurnal surface heating destabilized the troposphere east of the front. Also, a tongue of low-level moisture (≥20°C surface dewpoints) sustained the potential instability in central and eastern Texas. The 1735 UTC radar summary (Fig. 8a) shows thunderstorm activity ahead of the surface front. The deep convection organized into a line of thunderstorms by 2135 UTC (Fig. 8b).

The west–east cross section analysis of $\theta_v$, $r$, and wind vectors at 1200 UTC 22 (Fig. 9) shows a cold dome from west of Midland to east of Tucson, Arizona. Vertical wind shear (directional and speed) occurred at the eastern edge of the cold dome over Midland. The backing of wind with height through the front was consistent with the cold advection at ~4 km over Midland. Directional and speed shear also occurred at the western edge of the cold dome over Tucson, but veering with height was observed through the front, indicating a return of warmer air. A quasi-horizontal stable layer at ~6 km was observed from Midland to Longview, Texas, which contained little vertical wind shear. Between 8 and 9 km, a stable layer with significant vertical wind shear (~15 m s$^{-1}$/km) was observed between El Paso and Longview, suggesting the presence of a frontal feature. Several other interesting features within the cross section included 1) southwest winds east of the cold dome and west winds within the cold dome; 2) a pronounced stable layer east of the cold front at ~1.5 km MSL, which represented the capping boundary layer inversion or "lid" (Keyser and Carlson 1984), where moist Gulf or Mexico air ushered in on southeast winds was underlying dry desert plateau air from the southwest; and 3) a sharp horizontal moisture discontinuity at the surface cold front.

The northwest–southeast cross section analysis (Fig. 10) depicts a much deeper cold dome located northwest of the surface front. The two middle-tropospheric stable layers exhibited greater slopes and greater vertical wind shear in Fig. 10 than in Fig. 9. As in Fig. 9, Fig. 10 shows southwest winds in the warmer air and west winds in the cold dome. Moisture and temperature structure in the region of the lid and surface cold front are similar in the two figures.

The $\theta_v(t, z)$ analysis (Fig. 11) illustrates a number of features that were present over Midland during 22 April. A strong morning ground-based inversion was present until ~1200 UTC, the result of strong nocturnal radiational cooling. After 1200 UTC, a well-defined PBL formed. Between 1200 and 1430 UTC, the PBL growth rate was most rapid followed by less rapid vertical growth from 1430 to 1730 UTC. Strong surface heating is the primary mechanism by which the PBL grows during the day, the fastest growth occurring as solar insolation commences (e.g., see Panofsky and Dutton 1984). The top of the PBL ascended to a maximum height of ~4 km by 1730 UTC and remained at about 3.75 km for the rest of the period. The top of the PBL was capped by a narrow stable layer that ascended to ~4 km by 1715 UTC. After 1715 UTC, the top of the PBL was capped by a stable layer located between 4 and 4.5 km MSL. Superadiabatic conditions were present within the lowest kilometer during the growth of the PBL. Absolutely unstable conditions ($\partial\theta_v/\partial z < 0$) existed in the lowest 2 km of the PBL after this time. Adiabatic conditions were present from the top of the superadiabatic layer to the top of the PBL. In an unstable PBL, turbulent vertical mixing is driven primarily by strong surface heating and dry convection which is effective at trans-

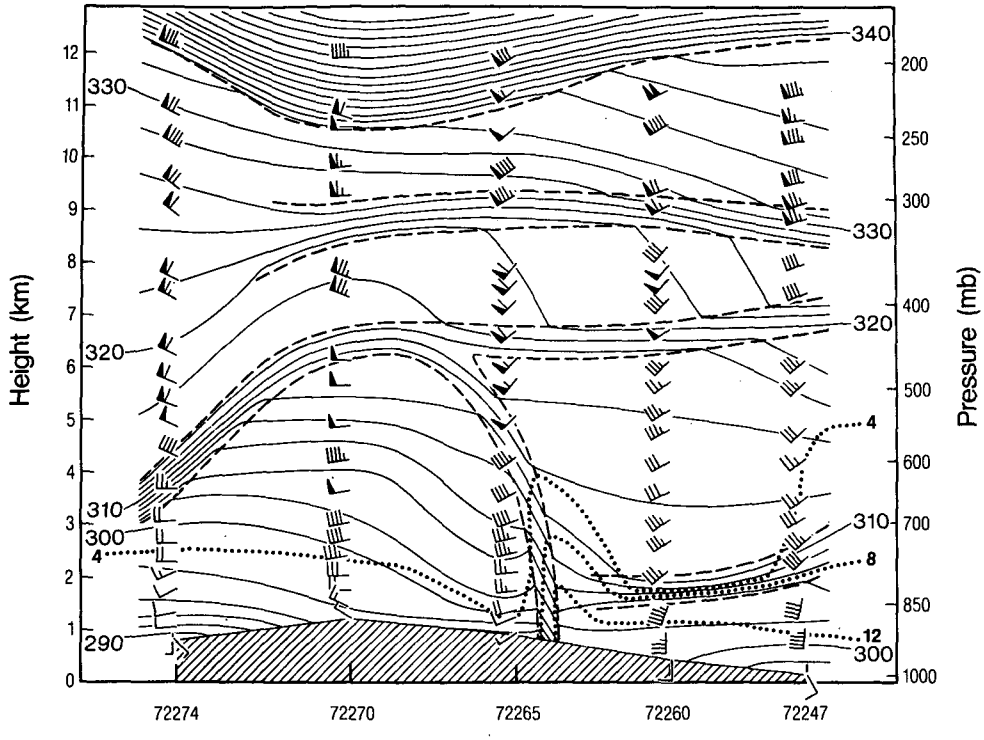


FIG. 9. Cross section of virtual potential temperature (K, solid lines), mixing ratio (g kg$^{-1}$, dotted lines), and wind vectors at 1200 UTC 22 April 1985; NWS rawinsonde data are from Tucson, Arizona (72274); El Paso (72270), Midland (72265), Stephenville (72260), and Longview, Texas (72247). Isentropes within dashed lines are stable layers, frontal layers, or the tropopause. Wind vectors are as decribed in Fig. 1.

porting stronger momentum toward ground level if $\partial V/\partial z > 0$ in the vicinity of the dry convection (Holton 1979). The rapid growth and unstable state of the PBL was an indication that dry convection was occurring within the PBL.

The $\theta_v(t, z)$ analysis (Fig. 11) shows several distinct stably stratified layers. One layer at ~7 km exhibited little temporal slope from 1100 to 1230 UTC before descending to ~4 km by 1915 UTC. The descent of isentropic warming in this layer was consistent with the eastward movement of the 500 mb thermal short wave and trailing warm front between 1200 UTC 22 and 0000 UTC 23 where a 4°C warming occurred at Midland. Thereafter, this stable layer, at just over 4 km, again exhibited little temporal slope. An ascending layer of isentropic cooling merged with the stable layer at 1200 UTC 22. The Midland surface observations indicated that a cold front, probably the ascending stable layer, intersected the ground at Midland at 0714 UTC. This front was the leading edge of the surface cold dome located over the western United States (Figs. 9 and 10).

At 1100 UTC, another elevated stable layer was observed just below 9 km and slowly descended to about 8.5 km by 1400 UTC. A more rapid descent of 3 km occurred between 1400 and 1800 UTC in response to the eastward movement of the thermal short wave. A slower descent of this layer occurred after 1800 UTC. The two descending stable layers merged between 1700 and 1830 UTC before separating again. The one ascending and two descending stable layers in Fig. 11 correspond to the ascending cold front and two midtropospheric frontal layers analyzed in the two cross sections (Figs. 9 and 10).

A stable layer with narrow vertical extend capped the growing PBL between 1230 and 1715 UTC. This layer did not appear to be associated with any frontal feature.

## 5. Lidar data analysis

Figure 12 presents the $t, z$ analysis of the lidar VAD and Midland rawinsonde wind profiles for the period 1115–2050 UTC 22 April 1985. The wind vectors above 650 mb show passage of the short wave as southwest winds shifted to west. The eastward progression of the short wave at 500 mb is shown in Figs. 5 and 6. Below 650 mb, the short-wave passage occurred prior to the start of the lidar $t, z$ analysis. The vertical speed shear layers (Fig. 12) generally coincided with the one temporally ascending and two temporally descending stable layers in the $\theta_v$ analysis (Fig. 11). From the geostrophic thermal wind relationship, which states that the strongest vertical shear is contained within vertically

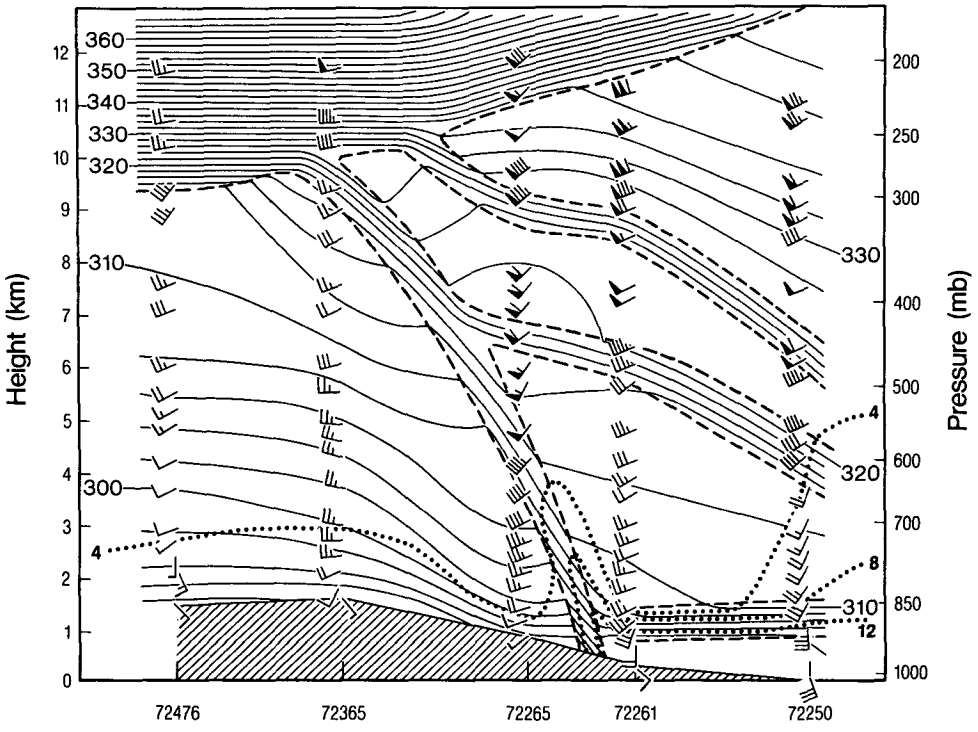


FIG. 10. Cross section of virtual potential temperature (K, solid lines), mixing ratio (g kg$^{-1}$), and wind vectors at 1200 UTC 22 April 1985; NWS rawinsonde data are from Grand Junction, Colorado (72476), Albuquerque, New Mexico (72365), Midland (72265), Del Rio (72261), Brownsville, Texas (72250). Isentropes within dashed lines are stable layers, frontal layers, or the tropopause. Wind vectors are as described in Fig. 1.

sloping (and usually thermally stable) baroclinic zones (Palmén and Newton 1969; Shapiro 1970), it can be concluded that the temporally ascending and descending stable layers (Fig. 11) were indeed frontal features. The ascending stable layer was the surface cold front that passed Midland at 0714 UTC, and the descending

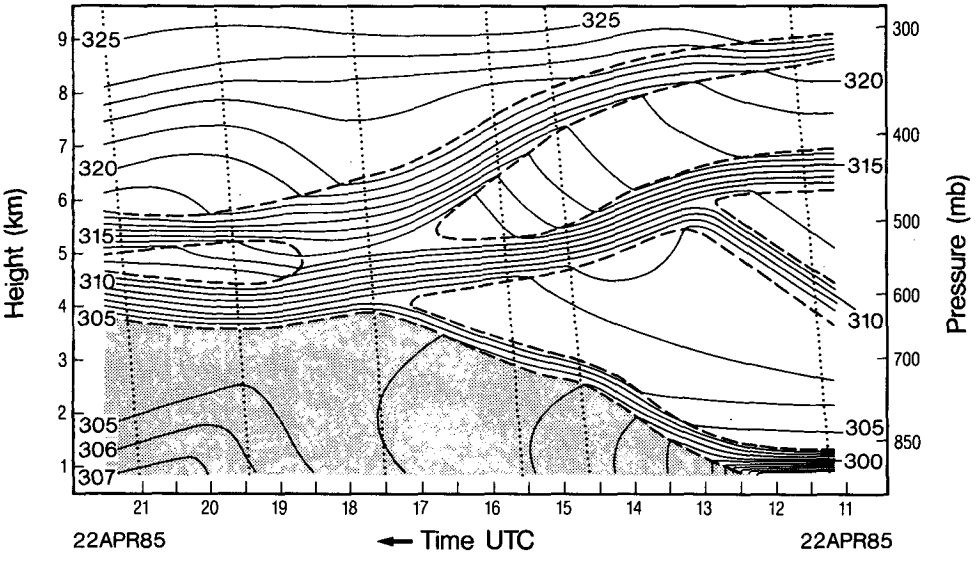


FIG. 11. Time–height section of virtual potential temperature (K) from 1115 to 2103 UTC 22 April 1985. Isentropes within dashed lines are stable layers or frontal layers. Dotted lines show rawinsonde launches adjusted with respect to time. Shaded area indicates region within the PBL.

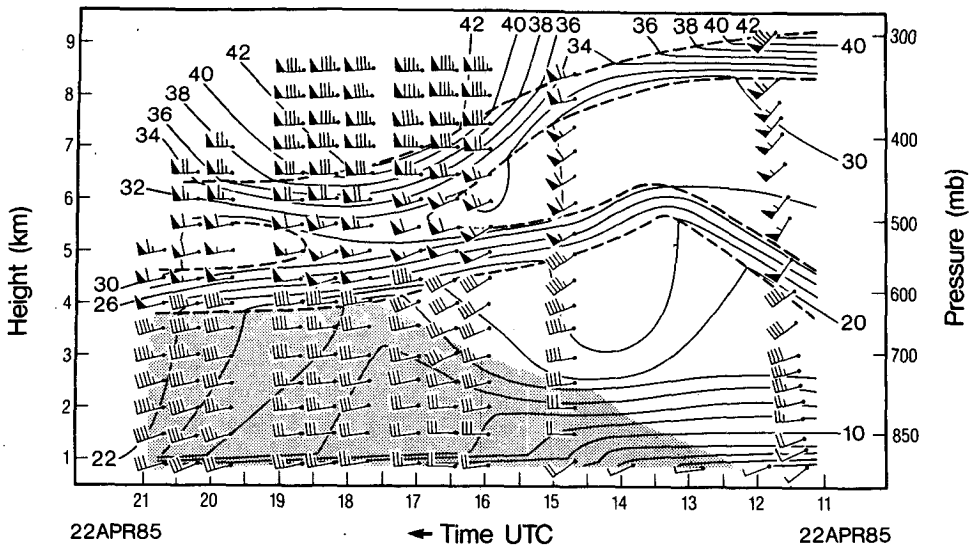


FIG. 12. Time–height section of filtered Doppler lidar horizontal winds (m $s^{-1}$) from 1442 to 2050 UTC 22 April 1985. The 1200 UTC Midland balloon launch data are included. Isotachs within dashed lines are enhanced vertical shear layers. Wind vectors are as described in Fig. 1. Shaded area indicates region within the PBL.

stable layers were midtropospheric warm fronts at the western edge of the eastward-moving cold dome. When a given stable layer contained no temporal slope, but still contained significant vertical shear, it was likely that the front had no phase velocity component normal to the temperature gradient over Midland. During the first 90 min of the $\theta_v$ time–height section, the stable layer near 6.5 km (Fig. 11) exhibited neither temporal slope nor vertical shear. The lack of vertical shear suggested that there was little horizontal baroclinity associated with the stable layer until after 1230 UTC.

Before 1730 UTC, Fig. 12 shows neither evidence of downward transport of strong westerly winds from turbulent mixing in the PBL nor a well-defined vertical shear layer at the top of the PBL. After 1730 UTC, the lidar isotach analysis showed the descent of stronger westerly winds into and within the PBL, at which time the top of the PBL was coincident with the bottom of the lower frontal vertical speed shear layer. It is likely that the strong winds and vertical wind shear associated with the frontal layer at ~4 km were transported to the surface by dry convective (turbulent) mixing, after the top of the PBL reached the frontal layer above. The downward transport of west winds or the downward momentum flux ($\overline{u'w'} < 0$) contributes to the local acceleration of westerly winds in the PBL when $\partial\overline{u'w'}/\partial z < 0$ (Holton 1979). Vertical profiles of $\overline{u'w'}$ were produced from the five 60° VAD wind profiles between 1635 and 1846 UTC 22 April using a conical scan technique (described by Eberhard et al. 1987). The three momentum flux profiles after 1730 UTC showed $\partial\overline{u'w'}/\partial z < 0$ from the top of the PBL into the lower frontal layer, indicating an acceleration of westerly winds into the PBL. The two $\overline{u'w'}$ profiles prior to 1730 UTC showed no such decrease with height, indicating a lack of west wind acceleration. These measurements concur with the isotach analysis in Fig. 12. Applying $K$ theory ($\partial\overline{u'w'}/\partial z = -K\partial^2 u/\partial z^2$) to the VAD wind profiles provided further evidence of the local west wind acceleration caused by the downward transport of west winds from the lower frontal layer into the PBL after 1730 UTC, when $\nabla^2 u > 0$ in this region. Strong backscatter signals taken from the VAD profiles (not shown) deepened with time from above ground level to ~4 km, such that the top of this layer was coincident with the top of the PBL (Figs. 11 and 12). Backscatter along the lidar beam is proportional to the number of aerosols in the atmosphere. Therefore, strong backscatter observed in the PBL was indicative of turbulent mixing, which transported dust from ground level to the top of the PBL and transported strong winds from the lower frontal layer into the PBL. It is speculated in McCarthy and Koch (1982) that zonal momentum in the midtropospheric jet stream could be entrained into the top of the PBL, then transported to the surface by turbulent mixing. The lidar observed a similar process, but in much greater detail, showing evidence of entrainment of strong winds from the frontal vertical shear layer into the top of the PBL, and the turbulent transport of those strong winds to the surface (Fig. 12). The warming of the cool air mass in western Texas and the corresponding weakening west–east temperature gradient at 850 mb support the suggestion that dry-convectively driven turbulence transported strong west winds down from the frontal shear layer.

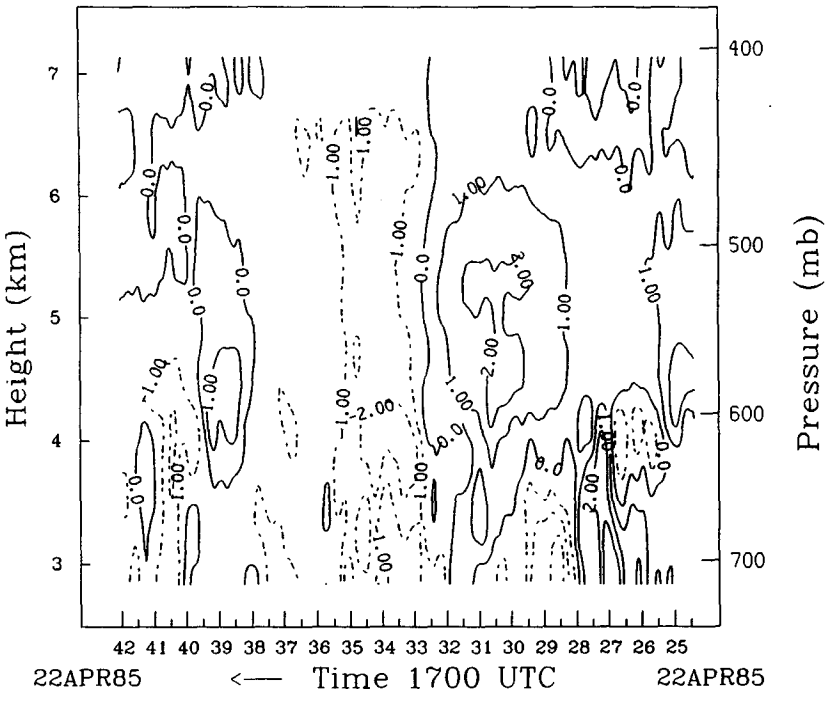


FIG. 13. Time–height section of vertical velocity (m $s^{-1}$) measured by the Doppler lidar from 1724–1742 UTC 22 April 1985.

The $t$, $z$ analysis of vertical velocity (1724–1742 UTC, Fig. 13) shows two distinct layers of vertical motion that differed significantly in character. The lower of the two layers (2.8–4.5 km MSL) contained large fluctuations in $W$ (from almost −4 to 4 m $s^{-1}$), indicating the presence of turbulence associated with dry convection in the PBL. The top of this turbulent layer coincided with the top of the PBL that extended to the base of both the capping stable layer in the $\theta_v$ time–height section (Fig. 11) and the base of the shear layer in the lidar isotach time–height section (Fig. 12). In the free atmosphere above 4.5 km, a less turbulent vertical velocity field was evident. A small increase in $W$ fluctuations occurred above 6 km.

The vertical profile of vertical velocity variance for the lowest detectable frequencies, [4.7–9.4 ($\times 10^{-4}$ $s^{-1}$)], revealed that the strongest signals were in the free atmosphere above 4 km (Fig. 14). Within the PBL, less energy was found in the low frequencies. The vertical profile of vertical velocity variance for the highest resolvable frequencies (0.14–0.224 $s^{-1}$) showed the strongest signals at 4.5 km and about 6.5 km (Fig. 15). The weakest signals were observed between 4.8 and 6 km. The high-frequency waves below 4 km were indicative of turbulence generated by the dry-convective overturnings in the PBL. The two turbulence maxima at 4.5 and 6.5 km may have been the result of clear air turbulence (CAT) generated by vertical shear instability within the frontal layers. The Richardson number profile calculated at 1733 UTC from Figs. 11 and 12 contained one local minimum of 1.051 at 4.45 km and another local minimum of 0.695 at 6.45 km (Fig. 15). The Ri profile was calculated from $\mathrm{Ri} = [N/(\partial \mathrm{V}/\partial z)]^2$, where $N$ is the Brunt–Väisälä frequency and $\partial \mathrm{V}/\partial z$ the total vertical wind shear. The vertical velocity variance profile for the smallest resolvable wavelengths was consistent with the Ri profile, where the minima and maxima of the first profile roughly coincided with the

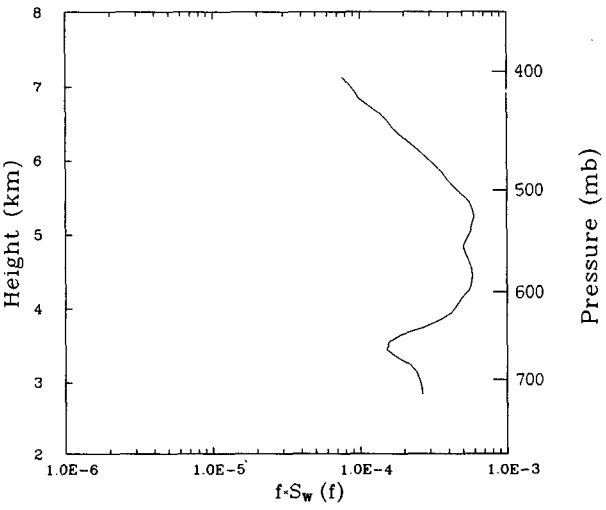


FIG. 14. Vertical profile of vertical velocity variance ($m^2$ $s^{-2}$) from lidar-measured $W$ for the frequency interval 4.7–9.4 ($\times 10^{-4}$ $s^{-1}$).

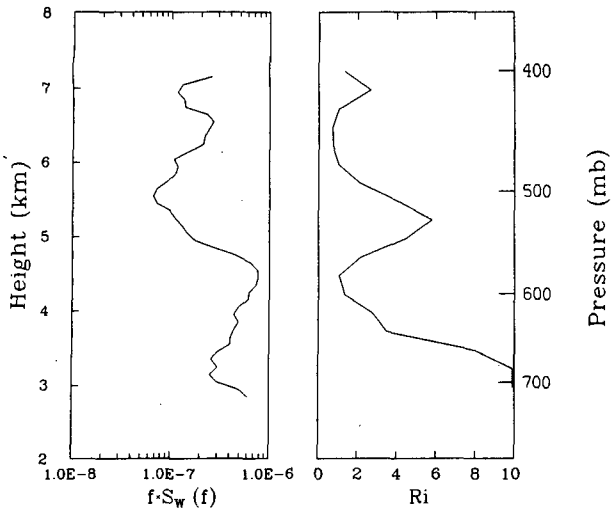


FIG. 15. As in Fig. 14 but for the frequency interval 0.14–0.224 $s^{-1}$, and the gradient Richardson number, Ri.

maxima and minima of the second profile (Fig. 15). Despite the fact that neither minimum in the Ri profile reached the critical value of Ri = 0.25 for shear instability and CAT, the fact that these two layers represented Ri minima suggested the greatest likelihood of CAT in these regions. Kennedy and Shapiro (1980) observed CAT in a frontal layer even though critical Ri values were not met for the total frontal layer. The implication of the subcritical Ri values calculated in the present study was that the vertical wind shear within the frontal layers may have been underestimated, because of smoothing of the lidar winds or a lack of vertical resolution of lidar wind measurements. Small-scale vertical shear layers (~100 m) may be supercritical (Ri $\leq$ 0.25), resulting in CAT even though the measured larger-scale shear layer (~1 km) in which they are embedded is subcritical. As a result, air can become turbulent when Ri > 0.25 for mesoscale perturbations (Panofsky and Dutton 1984). The lack of high-frequency waves between 4.8 and 6 km (the region of the Ri maximum) was consistent with the lidar velocity analysis showing a decrease in vertical shear in the layer (4.8–6.0 km) between the two frontal layers.

## 6. Conclusions

This study has shown another application of Doppler lidar technology to mesoscale and turbulent-scale meteorology. By coupling the lidar data with data from serial rawinsonde ascents, it has been shown that the lidar VAD scans are capable of measuring midtropospheric frontal systems as well as the high-frequency evolution of these systems. The VAD scans show the high temporal and vertical resolution structure of the winds in the PBL, such as the signature of downward transport of momentum. The vertical velocity scan is able to detect the high temporal variation of $W$ within the PBL and elevated frontal layers. It can also detect a more slowly varying $W$ in the free atmosphere. The vertical velocity variance profiles generated from lidar $W$ measurements are capable of detecting turbulence generated in the PBL, and CAT in the vicinity of frontal layers.

High-technology remote sensing instruments such as the Doppler lidar show considerable promise for future studies of small-scale weather systems. In a non-precipitating atmosphere, the ability of the lidar to detect short-term and small spatial variations will lead to new insights into topics such as velocity and turbulent structure of the PBL and frontal layers, and local circulations related to sea breezes, urban basins, canyon flows and mountain waves. Eventually, operational uses of the lidar could include 1) a ground-based network of lidars in the central United States to aid in the forecasting of severe convection, and 2) a space-based lidar network to retrieve global winds in data-sparse ocean regions.

Future papers will present the analysis of lidar measurements taken during 1) a severe downslope windstorm, showing a low-level jet and wind gust characteristics, 2) a dryline surge (during TEXEX), showing circulations about the discontinuity, and 3) a mountain lee wave flow pattern, showing perturbation wind features.

*Acknowledgments.* The men and women working at the National Weather Service Office at Midland, Texas are to be thanked for their cooperation and involvement with the Texas Frontal Experiment. The helpful comments of Dave Parsons of NCAR and John McGinley of PROFS are greatly appreciated. Their input enhanced the quality of this paper. The two anonymous reviewers also contributed valuable ideas.

## REFERENCES

Browning, K. A., and R. Wexler, 1968: The determination of kinematic properties of a wind field using Doppler radar. *J. Appl. Meteor.*, **7**, 105–113.

Eberhard, W. L., R. M. Hardesty and T. Gal-Chen, 1987: Turbulence measurements in the convective boundary layer with a short-pulse $CO_2$ Doppler lidar. Topical meeting on laser and optical remote sensing: Instrumentation and techniques, Sep. 28–Oct. 1, 1987, North Falmouth, MA, Optical Society of America, 1816 Jefferson Place, N. W., Washington, D. C., 20036, ThA5-1 to ThA5-4.

Hall, F. F., Jr., R. M. Huffaker, R. M. Hardesty, M. E. Jackson, T. R. Lawrence, M. J. Post, R. A. Richter and B. F. Weber, 1984: Wind measurement accuracy of the NOAA pulsed infrared Doppler lidar. *Appl. Opt.*, **23**, 1503–2506.

Hardesty, R. M., T. R. Lawrence, R. A. Richter, M. J. Post, F. F. Hall, Jr. and R. M. Huffaker, 1983: Ground-based coherent lidar measurement of tropospheric and stratospheric parameters. *Proc. SPIE*, **415**, 85–91.

Holton, J. R., 1979: *An Introduction to Dynamic Meteorology.* Academic Press, 391 pp.

Kennedy, P. J., and M. A. Shapiro, 1980: Further encounters with

clear air turbulence in research aircraft. *J. Atmos. Sci.*, **37**, 986–993.

Keyser, D., and T. N. Carlson, 1984: Transverse ageostrophic circulations associated with elevated mixed layers. *Mon. Wea. Rev.*, **112**, 2465–2478.

Lanczos, C., 1956: *Applied Analysis,* Prentice-Hall, 539 pp.

McCarthy, J., and S. E. Koch, 1982: The evolution of an Oklahoma dryline. Part I: A meso- and subsynoptic-scale analysis. *J. Atmos. Sci.*, **39**, 225–236.

Miller, J. E. 1948: On the concept of frontogenesis. *J. Meteor.*, **5**, 169–171.

Palmén, E., and C. W. Newton, 1969: *Atmospheric Circulation Systems,* Academic Press, 603 pp.

Panofsky, H. A., and J. A. Dutton, 1984: *Atmospheric Turbulence,* Wiley–Interscience, 397 pp.

Parsons, D. B., R. M. Hardesty and M. A. Shapiro, 1986: The mesoscale structure of the dryline and the formation of deep convection. *Int. Conf. on Monsoon and Mesoscale Meteorology,* Taiwan, Amer. Meteor. Soc., 117–122.

Post, M. J., and W. D. Neff, 1986: Doppler lidar measurement of winds in a narrow mountain valley. *Bull. Amer. Meteor. Soc.*, **67**, 274–281.

——, R. L. Schwiesow, R. E. Cupp, D. A. Haugen and J. T. Newman, 1978: Temporal and spatial frequency spectra for atmospheric aerosols. *J. Appl. Meteor.*, **17**, 1179–1181.

——, R. A. Richter, R. M. Hardesty, T. R. Lawrence and F. F. Hall, Jr., 1981: National Oceanic and Atmospheric Administration's (NOAA) Pulsed, Coherent, Infrared Doppler Lidar—Characteristics and data. *Proc. SPIE,* **300**, 60–65.

Rothermel, J., R. M. Hardesty and D. L. Davis, 1985: Dual-Doppler lidar measurement of winds in the JAWS Experiment. *J. Atmos. Oceanic Technol.*, **2**, 138–147.

Saucier, W. J., 1955: *Principles of Meteorological Analysis.* The University of Chicago Press, 438 pp.

Shapiro, M. A., 1970: On the applicability of the geostrophic approximation to upper-level frontal-scale motions. *J. Atmos. Sci.*, **27**, 408–420.

Velleman, P. F., and D. C. Hoaglin, 1981: *Applications, Basics, and Computing of Exploratory Data Analysis.* Duxbury Press, 384 pp.